NEURAL REGENERATION RESEARCH
www.nrronline.org

Research Article

Sustained release of exosomes loaded into polydopamine-modified chitin conduits promotes peripheral nerve regeneration in rats

https://doi.org/10.4103/1673-5374.335167

Date of submission: July 1, 2021

Date of decision: October 8, 2021

Date of acceptance: November 18, 2021

Date of web publication: February 8, 2022

Ci Li[1, 2, 3, #], Song-Yang Liu[1, 2, 3, #], Meng Zhang[1, 2, 3], Wei Pi[1, 2, 3], Bo Wang[4], Qi-Cheng Li[1, 2, 3], Chang-Feng Lu[1, 2, 3], Pei-Xun Zhang[1, 2, 3, *]

From the Contents

Graphical Abstract *Combined application of exosomes derived from bone marrow mesenchymal stem cells (BMSCs) and polydopamine-modified chitin conduit for repair of peripheral nerve injury*

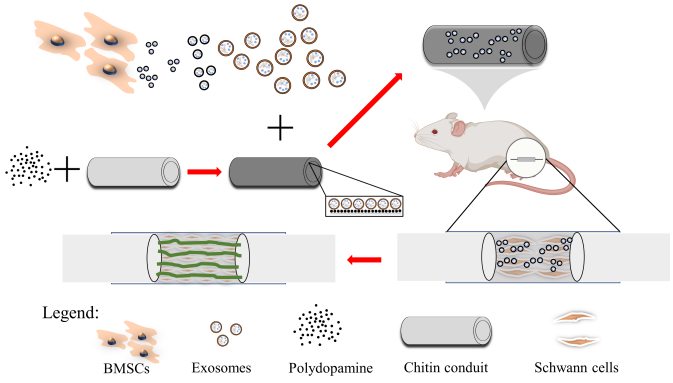

Abstract

Exosomes derived from mesenchymal stem cells are of therapeutic interest because of their important role in intracellular communication and biological regulation. On the basis of previously studied nerve conduits, we designed a polydopamine-modified chitin conduit loaded with mesenchymal stem cell-derived exosomes that release the exosomes in a sustained and stable manner. *In vitro* experiments revealed that rat mesenchymal stem cell-derived exosomes enhanced Schwann cell proliferation and secretion of neurotrophic and growth factors, increased the expression of *Jun* and *Sox2* genes, decreased the expression of *Mbp* and *Krox20* genes in Schwann cells, and reprogrammed Schwann cells to a repair phenotype. Furthermore, mesenchymal stem cell-derived exosomes promoted neurite growth of dorsal root ganglia. The polydopamine-modified chitin conduits loaded with mesenchymal stem cell-derived exosomes were used to bridge 2 mm rat sciatic nerve defects. Sustained release of exosomes greatly accelerated nerve healing and improved nerve function. These findings confirm that sustained release of mesenchymal stem cell-derived exosomes loaded into polydopamine-modified chitin conduits promotes the functional recovery of injured peripheral nerves.

Key Words: exosome; mesenchymal stem cells; modification strategy; nerve conduits; peripheral nerve injury; peripheral nerve regeneration; polydopamine; reprogramming state; Schwann cells; sustained release

Introduction

Peripheral nerve injury (PNI), which usually causes loss of function and decreased quality of life, is a worldwide medical problem (Jiang et al., 2017; Li et al., 2021). End-to-end neurorrhaphy is the conventional clinical therapy for small-gap peripheral nerve injuries; however, this technique has shortcomings, such as axonal misdirection and neuroma formation. Therefore, our team developed chitin (Chi) nerve conduits to bridge the nerve stumps as an alternative technique for neurorrhaphy (Zhang et al., 2013). A previous study reported that Chi was the ideal biomaterial to construct nerve conduits because of its antibacterial activity, biocompatibility, nontoxicity, and biodegradability (Lu et al., 2021). Compared with epineurium sutures, small-gap tubulization has significant advantages in shortening operation time, improving the accuracy of axonal docking, and reducing neuroma formation (Peixun et al., 2017). However, the hollow Chi conduits lack the biomechanical support and growth factors required for the initiation and maintenance of regeneration.

Schwann cells (SCs) are indispensable glial cells in the peripheral nervous system. The peripheral nervous system has better regeneration ability than the central nervous system, partly because SCs can reenter the cell cycle after receiving an injury

[1]Department of Orthopedics and Trauma, Peking University People's Hospital, Beijing, China; [2]Key Laboratory of Trauma and Neural Regeneration, Ministry of Education, Beijing, China; [3]National Center for Trauma Medicine, Beijing, China; [4]Department of Orthopedics, Beijing Jishuitan Hospital, Beijing, China
*Correspondence to: Pei-Xun Zhang, PhD, zhangpeixun@bjmu.edu.cn.
https://orcid.org/0000-0001-7200-2281 (Pei-Xun Zhang)
#Both authors contributed equally to this work.

Funding: *This study was supported by the National Natural Science Foundation of China, Nos. 31771322, 31571235; the National Science Foundation of Beijing, No. 7212121; Beijing Science Technology New Star Cross Subject, No. 2018019; Science and Technology Plan Project of Shenzhen, No. JCYJ 20190806162205278; the Key Laboratory of Trauma and Neural Regeneration (Peking University), Ministry of Education; and a grant from National Center for Trauma Medicine, No. BMU2020XY005-01 (all to PXZ).*

How to cite this article: *Li C, Liu SY, Zhang M, Pi W, Wang B, Li QC, Lu CF, Zhang PX (2022) Sustained release of exosomes loaded into polydopamine-modified chitin conduits promotes peripheral nerve regeneration in rats. Neural Regen Res 17(9):2050-2057.*

signal and dedifferentiate into a repair phenotype to support axon regeneration and remyelination (Lu et al., 2020; Nocera and Jacob, 2020; Castelnovo et al., 2021). Following PNI, SCs cooperate with macrophages to remove excess myelin debris, regulate the microenvironment, and support the survival of damaged neurons. Furthermore, SCs form Bünger bands to guide axonal regeneration and remyelination (Salzer, 2015; Jessen and Arthur-Farraj, 2019; Qu et al., 2021). Therefore, the activation and maintenance of the SCs' repair phenotype may be a way to repair PNI.

Over the years, exosomes derived from mesenchymal stem cells have attracted increasing attention in relation to stem cell-regulated therapeutic processes because they play a vital role in intercellular communication and biological regulation (Gnecchi et al., 2005; Timmers et al., 2007; Phinney et al., 2015). Exosomes are small (40–150 nm diameter) membrane vesicles that can be released by various cells. Exosomes contain multiple substances, such as functional proteins, lipids, DNA, mRNA, microRNA, and long non-coding RNA, which endow exosomes with some characteristics of primary cells (Valadi et al., 2007; Milane et al., 2015). Exosomes secreted by mesenchymal stem cells are used as therapy in regeneration fields such as skin wound healing (Xiao et al., 2021), bone regeneration (Zhang et al., 2020), and spinal cord injury restoration (Li et al., 2019). For faster nerve regeneration, it is important to use an appropriate delivery medium that not only preserves the bioactivity and bioavailability of exosomes but also easily bonds with Chi conduits.

The rapid development of biomaterial science has allowed various biomaterials to be widely used as therapies for PNI (Sensharma et al., 2017). Polydopamine (PDA), a mussel-inspired immobilization adhesive, has been widely used because of its high hydrophilicity, enduring adhesion ability, and excellent biochemical properties (Lee et al., 2007; Qian et al., 2018). Here, we modified Chi conduits using PDA and applied a combination of bone marrow mesenchymal stem cell-derived exosomes (BMSC-Exos) to repair 2 mm sciatic nerve defects in rats. We also investigated the biological effects of the PDA-coated conduits loaded with exosomes (Chi/PDA-Exos) on neural cells. The repair performance of these implanted conduits was evaluated by electrophysiological testing, locomotor functional recovery, and histological examination.

Materials and Methods

Cell culture and identification

Primary BMSCs were extracted from five male Sprague-Dawley rats at 28 days old, and primary SCs and dorsal root ganglias (DRGs) were extracted from five male Sprague-Dawley rats at 24 hours old, as previously described (Li et al., 2019; Rao et al., 2019, 2020). All rats were obtained from Beijing Vital River Laboratory Animal Technology Co. Ltd., Beijing, China (license No. SCXK (Jing) 2016-0006). All rats were anesthetized with ketamine (80 mg/kg; Zhong Mu Bei Kang Pharmaceutical Co. Ltd., Taizhou, China) and xylazine (10 mg/kg; Hua Mu Animal Health Products Inc., Changchun, China) by intraperitoneal injection, and then decapitated with sharp scissors. BMSCs were cultured and expanded in Dulbecco's Modified Eagle Medium/Nutrient Mixture F-12 (DMEM/F-12; Thermo Fisher Scientific, Waltham, MA, USA) with 10% fetal bovine serum (FBS; Thermo Fisher Scientific) and 1% penicillin/streptomycin (Beijing Solarbio Science & Technology Co. Ltd., Beijing, China). SCs were expanded in DMEM medium (Thermo Fisher Scientific) containing 10% FBS, 2 mM forskolin (MilliporeSigma, Burlington, MA, USA), and 2 ng/mL heregulin (MilliporeSigma). Then, SCs were cultured in DMEM with 10% FBS and 1% penicillin/streptomycin without any additives. DRGs were collected from the intervertebral foramen and cultured in DMEM/F-12 medium containing 10% FBS, 2% B-27 (Thermo Fisher Scientific), and 2 mM glutamine (Thermo Fisher Scientific). BMSCs, SCs, and DRGs were cultured in an incubator (Thermo Fisher Scientific) in a humidified atmosphere containing 5% CO_2 at 37°C. When the cells were 80% confluent, they were digested with trypsin (Thermo Fisher Scientific) for passaging.

Osteogenic, adipogenic, and chondrogenic stains were used to identify the differentiation abilities of BMSCs. After induction of osteogenic or adipogenic differentiation, BMSCs were fixed with 4% paraformaldehyde for 15–30 minutes at room temperature and washed with phosphate buffered saline (PBS; Solarbio). The cells were then stained with alizarin red S solution (an osteogenic marker; MilliporeSigma) or Oil Red O dye solution (an adipogenic marker; MilliporeSigma). For chondrogenic differentiation, 2×10^5 BMSCs were placed in a 15 mL sterile centrifuge tube and cultured in chondrogenic medium (Cyagen, Santa Clara, CA, USA) for 21 days. The differentiated cells were stained with alcian blue solution (MilliporeSigma) at room temperature for 0.5–1 hour in accordance with the manufacturer's instructions. Cells were rinsed with PBS and visualized using an optical microscope (Leica, Wetzlar, Germany).

A suspension of passage 2 BMSCs was prepared using trypsin (Thermo Fisher Scientific). After washing twice with PBS (Solarbio), BMSCs were collected by centrifugation. BMSCs were identified with Armenian hamster anti-CD29 (0.2 μg/10^6 cells, Cat# 102207; RRID: AB_312884, BioLegend, San Diego, CA, USA), rabbit anti-CD34 (1:50, Cat# bs-0646R; RRID: AB_10857521, Bioss Antibodies Inc., Woburn, MA, USA), mouse anti-CD45 (0.2 μg/10^6 cells, Cat# FITC-65064; RRID: AB_2883754, Proteintech Group, Inc., Rosemont, IL, USA), and mouse anti-CD90.1 (0.2 μg/10^6 cells, Cat# 11-0900-81; RRID: AB_465151, Thermo Fisher Scientific). After incubation with these antibodies for 1 hour, we analyzed the characteristics of BMSCs by flow cytometry (CytoFLEX; Beckman Coulter Inc., Brea, CA, USA). The identification of SCs and DRGs was confirmed and evaluated using specific antibodies in subsequent experiments.

Isolation and purification of exosomes

Exosomes were isolated using ultracentrifugation (Zhang et al., 2020). Briefly, the culture medium from passage 2–6 BMSCs was centrifuged at 300 × *g* for 10 minutes, 2000 × *g* for 10 minutes, and 10,000 × *g* for 30 minutes at 4°C. The collected supernatant was transferred to a new ultraclear tube (Beckman Coulter) and centrifuged at 100,000 × *g* for 70 minutes at 4°C. Finally, the precipitate in the centrifuge tube was collected and immediately stored in a –80°C freezer. The exosomes were identified by transmission electron microscopy (TEM; Philips, Amsterdam, Netherlands) and nanoparticle tracking analysis (NanoSight NS300; Malvern Panalytical, Malvern, UK). We analyzed the exosome markers rabbit anti-CD9 (1:1000, Cat# ab92726; RRID: AB_10561589, Abcam, Cambridge, UK), rabbit anti-CD63 (1:1000, Cat# PA5-92370; RRID: AB_2806456, Thermo Fisher Scientific), and rabbit anti-tumor susceptibility gene 101 (1:1000, TSG101, Cat# ab125011; RRID: AB_10974262, Abcam) by western blot assay.

Chi conduit modification

The method for Chi conduit fabrication has been patented (Chinese patent No. 01136314.2). First, the chitosan powder (MilliporeSigma) was diluted in 3% glacial acetic acid. We evenly covered a self-made mold with a diameter of 1.5 mm with the chitosan solution for 30 minutes at room temperature; then, the chitosan solution was solidified with 5% sodium hydroxide solution for 1 hour. Next, the chitosan conduits were removed from the mold, dried, and acetylated for 30 minutes. Finally, the Chi conduits were stored in 75% ethanol (Rao et al., 2019). The Chi conduits were cut into 6 mm lengths before PDA modification. Dopamine powder (MilliporeSigma) was diluted to a 2 mg/mL solution with 10 mM Tris buffer (pH 8.5). After the dopamine solution turned brown black, the prepared Chi conduits were immersed into PDA solution and were shaken at room temperature for 24 hours. The Chi/PDA conduits were washed with distilled water using an ultrasonic cleaner (SY-360; Jinli, Shanghai, China) until the water became clear to remove unattached dopamine molecules; the conduits were dried at room temperature for use in further experiments.

Exosome immobilization, observation, and sustained release rates

Exosomes were immobilized by immersion of one Chi conduit and one Chi/PDA conduit in 1 mg/mL exosome solution with mild shaking for 12 hours at 4°C. Image of untreated Chi conduits and images of the distribution of exosomes on exosome-treated Chi (Chi-Exos) conduits and Chi/PDA (Chi/PDA-Exos) conduits were acquired with a scanning electron microscope (JSM-6700F; JEOL Ltd., Tokyo, Japan).

The loading qualities and release rates of BMSC-Exos were measured using an ultraviolet-visible-near-infrared spectrophotometer (UV-2450; Shimadzu Corporation, Kyoto, Japan). Briefly, Chi-Exos (n = 3) and Chi/PDA-Exos (n = 3) conduits were placed in six tubes that each contained 500 μL 1× PBS solution. Each tube was kept slowly shaking at 37°C. At predetermined time points, the supernatants of different samples were collected to quantify the release rates of BMSC-Exos from the conduits.

Bone marrow mesenchymal stem cell-derived exosomes labeling and uptake assay

BMSC-Exos were labeled with the red-fluorescent dye PKH26 (MilliporeSigma) in accordance with the manufacturer's instructions. Chi and Chi/PDA conduits were incubated in a solution of PKH26-labeled exosomes for 12 hours. Next, SCs were seeded at a density

of 5 × 10^5 cells per well in six-well plates and treated with Chi-Exos or Chi/PDA-Exos conduits for 1 or 5 days. Subsequently, the SCs were labeled with fluorescein isothiocyanate-labeled phalloidin (MilliporeSigma) and 4′,6-diamidino-2-phenylindole (MilliporeSigma). Immunofluorescence images were captured with a laser confocal scanning microscope (Leica).

Neural cell immunofluorescence

Immunofluorescence was used to visualize the biological effects of different conduits on SCs and DRGs. Briefly, DRGs were treated in the same way as SCs. Each group of three DRGs was placed in six-well plates and treated with Chi, Chi-Exos, Chi/PDA, or Chi/PDA-Exos for 7 days. On the 5th day after treatment for SCs and the 7th day after treatment for DRGs, the SC and DRG samples were washed with PBS three times and fixed with 4% paraformaldehyde for 15 minutes. Rabbit anti-S100 antibody (a specific marker of SCs, 1:400, RRID: AB_477501, Cat# S2644; MilliporeSigma) and mouse anti-neurofilament 200 (a specific marker of DRGs, 1:400, RRID:AB_477257, Cat# N0142; MilliporeSigma) were incubated overnight at 4°C with SCs and DRGs, respectively. Goat anti-rabbit IgG (RRID: AB_2650602, Cat# ab150080; Abcam) and goat anti-mouse IgG (RRID: AB_2576208, Cat# ab150113; Abcam) were then incubated with the SCs and DRGs, respectively, in the dark for 1 hour at room temperature. Finally, the nuclei of SCs were labeled with 4′,6-diamidino-2-phenylindole. A fluorescence microscope (Leica) was used to observe and photograph three SC and DRG samples in each group for statistical analysis. The number of SCs and the mean length of each DRG axon were measured with ImageJ 1.51j8 software (National Institutes of Health, Bethesda, MD, USA) (Schneider et al., 2012).

Schwann cell proliferation

SC proliferation was assessed with the Cell Counting Kit-8 (CCK-8; Dojindo, Kumamoto, Japan). Briefly, primary SCs at 5 × 10^5 cells per well were seeded in six-well plates and incubated overnight at 37°C before Chi-Exos or Chi/PDA-Exos conduits were added. On the 1st and 5th days after treatment, CCK-8 working solution was added to each well and incubated for 2 hours. After that, 100 μL supernatant was transferred into a new 96-well plate and measured with a microplate reader (Bio-Rad Laboratories, Hercules, CA, USA). Each sample was tested three times.

Enzyme-linked immunosorbent assay

To determine whether the BMSC-Exos affected SC protein secretion, the supernatants of SCs treated with Chi, Chi/PDA, Chi-Exos, or Chi/PDA-Exos were collected on the 1st and 5th days after treatment. Nerve growth factor, brain-derived neurotrophic factor, ciliary neurotrophic factor, and vascular endothelial growth factor were measured with enzyme-linked immunosorbent assay (ELISA) kits (Abcam). Absorbance at 450 nm was measured with a microplate reader (Bio-Rad). Each sample was tested three times.

Reverse transcription-polymerase chain reaction analysis

To determine phenotypic differentiation, total RNA was extracted from SCs treated with Chi, Chi/PDA, Chi-Exos, or Chi/PDA-Exos on the 1st and 5th days after treatment using TRIzol reagent (Thermo Fisher Scientific). The primer sequences are listed in **Table 1**. Gapdh was used as the internal control. Cycling conditions were as follows: 30 seconds at 95°C, followed by 40 cycles of 5 seconds at 95°C, 10 seconds at 55°C, and 15 seconds at 72°C. The data was recorded by the real-time polymerase chain reaction system (Applied Biosystems, Waltham, MA, USA). The relative gene expression was analyzed by the Livak method (Schmittgen and Livak, 2008).

Table 1 | **Primer sequences for reverse transcription-polymerase chain reaction**

Gene	Forward primer (5'–3')	Reverse primer (5'–3')
Jun	GGG TGC CAA CTC ATG CTA ACG	TCT CTG TCG CAA CCA GTC AAG T
Sox2	CCA GCT CGC AGA CCT ACA TGA A	GCC TCG GAC TTG ACC ACA GA
MBP	GCT GCC GAA GGT CAC CAT CT	AGC ACG AGG CCA CCA GAG AA
Krox20	GAC CAC CTC ACC ACT CAC ATC C	GGC ACT GCT CTT CCT CTC CTT C
Gapdh	GCC ATC ACT GCC ACT CAG AAG A	ATG ACC TTG CCC ACA GCC TTG

Gapdh: Glyceraldehyde-3-phosphate dehydrogenase; Krox20: also known as EGR2, early growth response 2; MBP: myelin basic protein; Sox2: SRY-related HMG-box 2.

Animals and surgical procedures

The study protocol was approved by the Medical Ethics Committee of Peking University People's Hospital on December 5, 2019 (approval No. 2019PHE027). There are sex-related differences in collateral sprouting of axons after PNI (Kovacic et al., 2003). To eliminate these differences and aggressive behavior in male rats, we used female rats as the experimental animals. Thirty-two specific-pathogen-free female Sprague-Dawley rats (weighing 200–220 g and aged 6–8 weeks) were obtained from the Beijing Vital River Laboratory Animal Technology Co. Ltd. All rats were evenly and randomly divided into four groups (n = 8 rats per group): Chi, Chi-Exos, Chi/PDA, and Chi/PDA-Exos groups. All rats were anesthetized with 5 L/min isoflurane (Zhong Mu Bei Kang Pharmaceutical Co. Ltd.) inhalation, and the anesthesia was maintained with 2 L/min isoflurane inhalation. The hair of the right hind limb of the rat was shaved using a razor, and the skin was disinfected with iodophor. The right sciatic nerve was exposed and transected 7 mm above the sciatic nerve fork. The nerve stumps were bridged with nerve grafts under a surgical microscope (Leica) using 10-0 nylon sutures, and a 2 mm gap was kept between the nerve stumps. The muscles and skin were sutured after careful disinfection. Rats were provided with food and water ad libitum.

Behavioral analysis

We used the CatWalk XT 10.6 gait analysis system (Noldus, Wageningen, Netherlands) to analyze the motor function recovery of all rats in each group 8 weeks after surgery. After the rats were familiar with the track environment, a high-speed camera (Noldus) was used to record the footprints of the rats during the gait test. The sciatic functional index (SFI) evaluated the motor function of the rats and was calculated using the following formula (Rao et al., 2020): SFI = 109.5(ETS–NTS)/(NTS)–38.3(EPL–NPL)/(NPL) + 13.3(EIT–NIT)/NIT–8.8, where ETS is the experimental toe spread and NTS is the normal toe spread (distance from the first to the fifth toe), EPL is the experimental paw length and NPL is the normal paw length (distance from the heel to the top of the third toe), and EIT is the experimental intermediary toe spread and NIT is the normal intermediary toe spread (distance from the second to the fourth toe).

Electrophysiological examination

Eight weeks after surgery, we used the compound motor action potential (CMAP) to assess sciatic nerve conduction for three rats in each group. Briefly, one stimulating electrode was placed 5 mm from the proximal ends of the nerve conduits. Two recording electrodes were attached: one on the proximal side and one on the distal side of the gastrocnemius muscle. A rectangular pulse (stimulus intensity 0.9 mA, pulse duration 0.1 ms) was used to stimulate the sciatic nerve. Then, latency and amplitude of the CMAPs were recorded using an electrophysiological instrument (Oxford Instruments, Oxford, UK).

Neurohistological analysis

Regenerated nerve tissues were collected 8 weeks after surgery. All rats were euthanized by carbon dioxide inhalation with a filling rate of 30–70% per minute. The distal 2 mm of the regenerated nerve was fixed with 2.5% glutaraldehyde (MilliporeSigma), stained with 1% osmium tetroxide (MilliporeSigma), and embedded in epoxy resin. The specimens were cut into 700 nm semithin slices and 70 nm ultrathin sections. An optical microscope (Leica) was used to observe the myelinated nerve fiber densities on semithin sections after staining with 1% toluidine blue (MilliporeSigma). The ultrathin sections were dyed with uranyl acetate and lead citrate. We measured the thicknesses of the newly formed myelin sheaths and the diameters of the remyelinated axons in three random areas by TEM (Philips).

Gastrocnemius muscle weight and muscle histological analysis

The gastrocnemius muscles were isolated from both hind limbs 8 weeks after sciatic nerve surgery. The muscle specimens were immediately weighed with an electronic balance (Mettler Toledo, Greifensee, Switzerland). The wet weight rate was obtained using the following equation: Wet weight rate = w/W × 100%, where w is the wet weight of the operated muscle, and W is the wet weight of the unoperated muscle. The muscle specimens were fixed in 4% paraformaldehyde and embedded in paraffin. The middle section of the gastrocnemius muscle was cut into 5 μm thick sections and subjected to Masson's trichrome staining (Solarbio). We observed cross sections of the gastrocnemius muscle fibers in three random areas through an optical microscope; ImageJ was used to quantify and analyze the cross-sectional areas of the muscle fibers.

Statistical analysis

We selected 6–8 rats as the sample size for our studies, based on other publications on nerve injury and regeneration (Rao et al., 2019, 2020). The data evaluator was blinded to the rat groupings. All data were calculated as the mean ± standard error of the mean (SEM) and were analyzed using GraphPad Prism, version 7.04 (GraphPad Software, San Diego, CA, USA). One-way analysis of variance was used for differences between multiple groups, and then Tukey's *post hoc* test was applied. In all analyses, $P < 0.05$ was considered statistically significant.

Results

Characterization of bone marrow mesenchymal stem cells and bone marrow mesenchymal stem cell-derived exosomes

Optical microscope images demonstrated that BMSCs had spindle morphology (**Figure 1A**). After induction of differentiation, calcium deposits inside and outside the cells appeared red after alizarin red staining (**Figure 1B**). Red lipid droplets were found in BMSCs after Oil red O staining (**Figure 1C**). **Figure 1D** shows the round morphology typical of chondrocytes. Flow cytometry (**Figure 1E**) showed that CD29 and CD90 were positive (both > 95%) and CD34 and CD45 were negative (both < 5%). In conclusion, the cells used in our experiments met the characteristics of BMSCs.

TEM analysis showed that the exosomes isolated from the supernatants of BMSCs had a typical lipid bilayer membrane and cup-shaped morphology (**Figure 1F**). Nanoparticle tracking analysis revealed that the exosomes were 110.3 ± 2.6 nm in diameter (**Figure 1G**). The specific exosome markers CD9, CD63, and TSG101 were positive (**Figure 1H**).

Morphological analysis and release kinetics of exosomes from different conduits *in vitro*

Chi conduits were nearly transparent, while the Chi/PDA conduits had low transparency and appeared black (**Figure 2A** and **B**). Chi-Exos and Chi/PDA-Exos conduits were constructed by immersing Chi and Chi/PDA conduits in BMSC-Exos solution (**Figure 2C**). A scanning electron microscope was used to observe the number and morphology of exosomes on the surface of Chi and Chi/PDA conduits. The Chi conduit was composed of many disordered micron-scale Chi fibers (**Figure 2D**). More BMSC-Exos were distributed on the surface of Chi/PDA conduits than Chi conduits ($P < 0.01$; **Figure 2E** and **F**). The exosome-loading qualities of Chi and Chi/PDA conduits were 346.7 ± 8.82 μg and 710 ± 17.32 μg, respectively (**Figure 2G**). Furthermore, the sustained-release experiment demonstrated that exosomes were burst released from Chi conduits in the first 48 hours, and few exosomes were detected after 10 days. In contrast, there was a pattern of sustained release of immobilized exosomes from Chi/PDA conduits within 14 days. Approximately 22.56 ± 2.42% of the exosomes remained in the Chi/PDA conduits after 14 days (**Figure 2H** and **I**).

Chi/PDA-Exos provides more exosomes than Chi-Exos

On the 1st day after treatment, we found that the area of PKH26-labeled BMSC-Exos in the phalloidin-labeled SCs of the Chi-Exos group was larger than that of the Chi/PDA-Exos group ($P < 0.01$). On the 5th day after treatment, the area of PKH26-labeled BMSC-Exos was smaller in the Chi-Exos group than in the Chi/PDA-Exos group ($P < 0.01$; **Figure 3A** and **B**).

Chi/PDA-Exos improve Schwann cell proliferation and secretory capacity and activates the reprogramming process

On the 5th day after treatment, the SCs in the Chi-Exos and Chi/PDA-Exos groups had elongated bipolar fusiform morphology, which is consistent with the typical morphology of repaired SCs, but the SCs in the other groups were comparatively flat (**Figure 4A**). CCK-8 results showed proliferation of SCs was highest in the Chi-Exos group 1 day after treatment ($P < 0.05$, *vs*. Chi group) (**Figure 4B**). On the 5th day after treatment, Chi/PDA-Exos gave an obvious advantage in promoting SC proliferation ($P < 0.01$, *vs*. Chi-Exos group) (**Figure 4B**).

The protein expression of three neurotrophic factors (nerve growth factor, brain-derived neurotrophic factor, and ciliary neurotrophic factor) and vascular endothelial growth factor was analyzed by ELISA. On the 1st day after treatment, we found that SCs in the Chi-Exos group secreted higher levels of neurotrophic factors and vascular endothelial growth factor than SCs in the other three groups ($P < 0.05$). Chi/PDA-Exos gave excellent regulation of SC secretory function 5 days after treatment (**Figure 4C–F**).

The expression levels of the repair-phenotype marker genes (*Jun* and *Sox2*) and myelin-related genes (*Mbp* and *Krox20*) were evaluated by reverse transcription-polymerase chain reaction. No significant difference was found in the genes' expression levels in SCs treated with Chi or Chi/PDA ($P > 0.05$), while exosome treatment upregulated the mRNA expression levels of *Jun* and *Sox2* and downregulated the mRNA expression levels of *Mbp* and *Krox20* on the 1st day after treatment ($P < 0.05$). PDA also increased the mRNA expression of *Mbp* and *Krox20* on the 5th day after treatment. The sustained release of exosomes continued to activate the SC repair phenotype ($P < 0.05$; **Figure 4G–J**).

Chi/PDA-Exos enhance neurite growth of dorsal root ganglia

Immunofluorescence staining was performed to evaluate the effect of Chi/PDA-Exos on DRG neurites (**Figure 5A**). On the 7th day, the average length of DRG neurites treated with Chi-Exos, Chi/PDA, or Chi/PDA-Exos was significantly increased compared with the Chi group ($P < 0.01$; **Figure 5B**).

Chi/PDA-Exos promote motor function and electrical conduction recovery *in vivo*

Rat footprints and the SFI rating scale were used to evaluate functional recovery of PNI up to 8 weeks after surgery. Results revealed unambiguous footprints with better toe spread in the Chi/PDA-Exos group compared with other groups (**Figure 6A**). The SFI value of the Chi/PDA-Exos group was clearly superior to the Chi and Chi-Exos groups 8 weeks postoperation ($P < 0.01$; **Figure 6B**).

Eight weeks after surgery, sciatic nerve conduction of all groups was examined. The CMAP latency of the Chi/PDA-Exos group was lower than the Chi group ($P < 0.01$) and was similar to the Chi-Exos group ($P > 0.01$). The CMAP amplitude of the Chi/PDA-Exos group was higher than the Chi and Chi-Exos groups ($P < 0.01$; **Figure 6C–E**).

Eight weeks after surgery, we observed different degrees of atrophy of the gastrocnemius muscle on the operated side (**Figure 6F**). The wet weight rate of the gastrocnemius muscle in the Chi/PDA-Exos group was significantly higher than in the Chi and Chi-Exos groups ($P < 0.05$; **Figure 6G**). As shown in **Figure 6H** and **I**, Masson's trichrome staining showed that the cross-sectional area of the muscle fiber in the Chi/PDA-Exos group was larger than in the Chi and Chi-Exos groups ($P < 0.05$).

Chi/PDA-Exos improve sciatic nerve regeneration and remyelination *in vivo*

Eight weeks after surgery, the regenerated sciatic nerve was exposed and evaluated. SC myelination plays a critical role in axonal regeneration after PNI (Nocera and Jacob, 2020). Toluidine blue staining was performed 8 weeks post-implantation (**Figure 7A**). TEM was performed to evaluate the myelin sheath thickness and the diameter of regenerated myelinated nerve fibers (**Figure 7B**). Compared with the Chi group, the numbers of axons at the distal ends of the regenerating nerve bundles were increased significantly in the Chi-Exos and Chi/PDA groups, and especially in the Chi/PDA-Exos group (**Figure 7C**). TEM showed that the laminated myelin sheaths of regenerated nerve fibers in the Chi-Exos and Chi/PDA groups were greater than in the Chi group ($P < 0.05$). We also found the mean diameter of regenerated axons in the Chi/PDA-Exos group was the largest compared with the other groups (**Figure 7D–E**).

Discussion

Currently, neurorrhaphy is a common technique to repair small-gap peripheral nerve defects (Pabari et al., 2010). However, complications, such as misconnection of nerve fibers, are difficult to avoid. Peripheral nerve conduits take advantage of nerve fiber chemotaxis to achieve better therapeutic effects (Zhang et al., 2015, 2019). However, hollow Chi conduits lack the biomechanical support or growth factors required to promote regeneration. Meanwhile, proximal axons need enough space to self-connect with the distal target tissues. Therefore, it is important to develop a proper strategy that can promote not only promote nerve regeneration but also nerve self-docking.

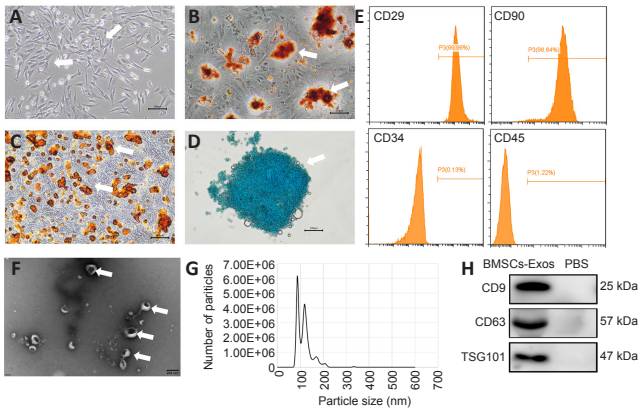

Figure 1 | Identification of BMSCs and BMSC-Exos.
(A) Representative spindle shape (white arrows) of BMSCs. (B) Alizarin red staining shows calcium nodules (white arrows) after osteogenic differentiation. (C) Oil red O staining shows lipid droplets (white arrows) after adipogenic differentiation. (D) Alcian blue staining shows a chondrocyte group (white arrow) after chondrogenic differentiation. Scale bars: 100 μm (A–D). (E) Flow cytometric analysis of surface markers of BMSCs. The BMSCs were positive for CD29 and CD90 and negative for CD34 and CD45. (F) Representative morphology of BMSC-Exos (white arrows) observed by transmission electron microscopy. Scale bar: 200 nm. (G) Particle size distribution in purified BMSC-Exos measured by nanoparticle tracking analysis. (H) Western blot analysis of the specific exosome surface markers CD9, CD63, and TSG101. BMSCs: Bone mesenchymal stem cells; BMSCs-Exos: exosomes derived from bone mesenchymal stem cells; PBS: phosphate buffered saline; TSG101: tumor susceptibility gene 101.

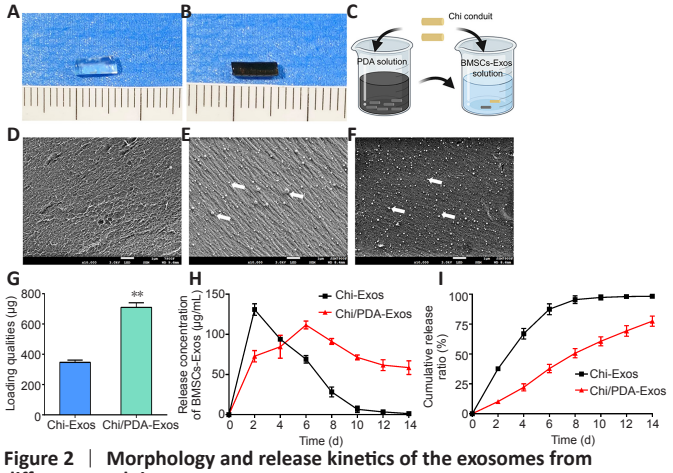

Figure 2 | Morphology and release kinetics of the exosomes from different conduits.
(A, B) Gross view of the Chi conduit without (A) or with (B) PDA. Scale bars: 1 mm. (C) Schematic illustration of preparation of Chi-Exos and Chi/PDA-Exos conduit. (D) Transmission electron microscopy image of the surface morphology of Chi conduits. (E, F) Distribution of exosomes (white dots; identified by the white arrows) on the Chi-Exos (E) and Chi/PDA-Exos conduits (F). Scale bars: 1 μm (D–F). (G) Quantitative analysis of loading qualities of BMSC-Exos in Chi-Exos and Chi/PDA-Exos conduits. (H, I) Quantitative analysis of BMSC-Exos release and kinetics from Chi-Exos and Chi/PDA-Exos conduits. Data are expressed as mean ± SEM (n = 3 for each group). $^{**}P < 0.01$, *vs.* Chi-Exos group (one-way analysis of variance followed by Tukey's *post hoc* test). BMSCs-Exos: Exosomes derived from bone mesenchymal stem cells; Chi: chitin; Chi/PDA-Exos: polydopamine-coated chitin conduits loaded with exosomes; Chi-Exos: chitin conduits loaded with exosomes; Exos: exosomes; PDA: polydopamine.

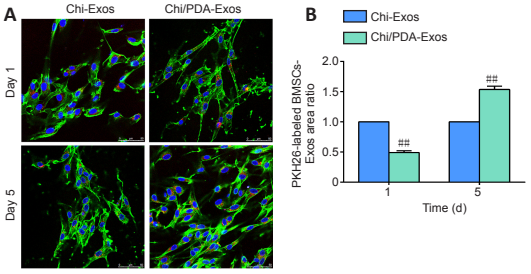

Figure 3 | Chi/PDA-Exos provide more exosomes than Chi-Exos.
(A) SCs (green, FITC) were treated with PKH26-labeled BMSC-Exos (red) in Chi-Exos and Chi/PDA-Exos conduits for 1 and 5 days. On the 1st day after treatment, the area of PKH26-labeled BMSC-Exos (red dots) in the phalloidin-labeled SCs (green cells) in the Chi-Exos group was larger than in the Chi/PDA-Exos group. On the 5th day after treatment, the area of PKH26-labeled BMSC-Exos was smaller in the Chi-Exos group than in the Chi/PDA-Exos group. Scale bars: 50 μm. (B) Quantification analysis of relative fluorescence area ratio of SCs that internalized BMSC-Exos. $^{\#\#}P < 0.05$, *vs.* Chi-Exos group (one-way analysis of variance followed by Tukey's *post hoc* test). BMSCs-Exos: Exosomes derived from bone mesenchymal stem cells; Chi: chitin; Chi/PDA: polydopamine-coated chitin conduits; Chi/PDA-Exos: polydopamine-coated chitin conduits loaded with exosomes; Chi-Exos: chitin conduits loaded with exosomes; FITC: fluorescein isothiocyanate.

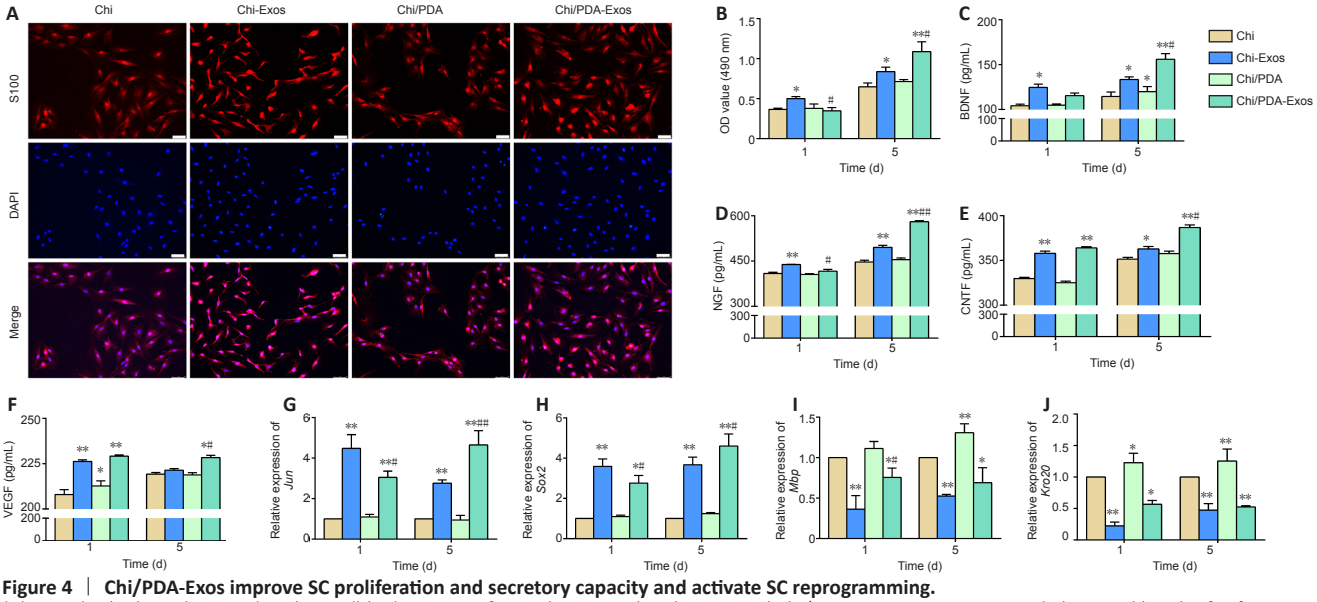

Figure 4 | Chi/PDA-Exos improve SC proliferation and secretory capacity and activate SC reprogramming.
(A) S100 (red, Alexa Fluor 594) and DAPI (blue) staining of SCs. The SCs in the Chi-Exos and Chi/PDA-Exos groups presented elongated bipolar fusiform morphology, but the SCs in the other groups were relatively flat. Scale bars: 50 μm. (B) SC proliferation was evaluated using the Cell Counting Kit-8 assay. (C–F) BDNF, NGF, CNTF, and VEGF secreted from SCs were detected by enzyme-linked immunosorbent assay. Data are expressed as mean ± SEM (n = 3 for each group). (G–J) Quantitative analysis of *Jun*, *Sox2*, *Mbp*, and *Krox20* mRNA levels in SCs (reverse transcription-polymerase chain reaction). mRNA levels were normalized to the Chi group. Data are expressed as mean ± SEM (n = 3 for each group). $^{*}P < 0.05$, $^{**}P < 0.01$, *vs.* Chi group; $^{\#}P < 0.05$, $^{\#\#}P < 0.05$, *vs.* Chi-Exos group (one-way analysis of variance followed by Tukey's *post hoc* test). BDNF: Brain-derived neurotrophic factor; Chi: chitin; Chi/PDA: polydopamine-coated chitin conduits; Chi/PDA-Exos: polydopamine-coated chitin conduits loaded with exosomes; Chi-Exos: chitin conduits loaded with exosomes; CNTF: ciliary neurotrophic factor; DAPI: 4′,6-diamidino-2-phenylindole; Krox20: also known as EGR2, early growth response 2; MBP: myelin basic protein; NGF: nerve growth factor; SCs: Schwann cells; Sox2: SRY-related HMG-box 2; VEGF: vascular endothelial growth factor.

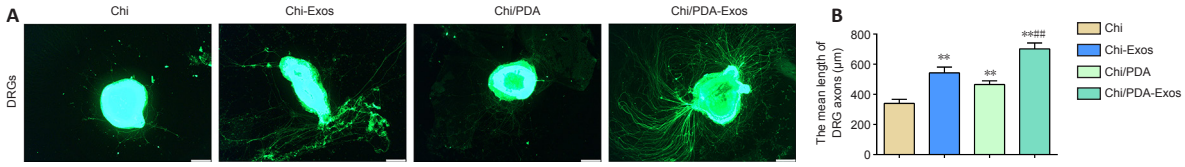

Figure 5 | **Chi/PDA-Exos enhances neurite growth of DRGs after 7 days of treatment.**
(A) BMSC-Exos enhanced the length of DRGs axon (green, Alexa Fluor 488) tested with different conduits. The length of the DRG axons was markedly increased by treatment with Chi/PDA-Exos compared with Chi alone. Scale bars: 50 μm. (B) Quantification analysis of DRG axon length. Data are expressed as mean ± SEM (n = 3 for each group). $^{**}P < 0.01$, *vs.* Chi group; $^{\#\#}P < 0.01$, *vs.* Chi-Exos group (one-way analysis of variance followed by Tukey's *post hoc* test). Chi: Chitin; Chi/PDA: polydopamine-coated chitin conduits; Chi/PDA-Exos: polydopamine-coated chitin conduits loaded with exosomes; Chi-Exos: chitin conduits loaded with exosomes; DRGs: dorsal root ganglions.

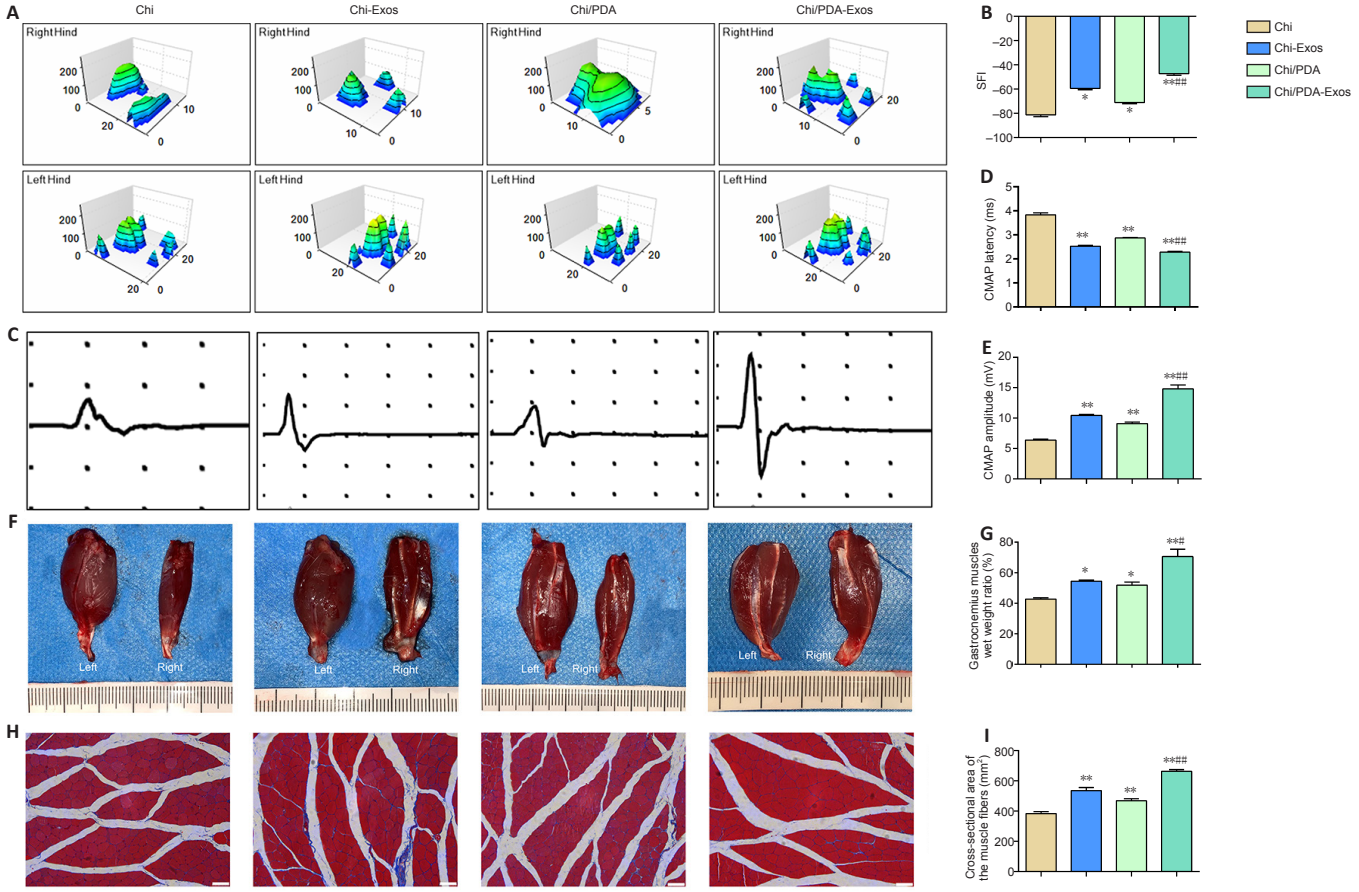

Figure 6 | **Chi/PDA-Exos improve functional recovery and gastrocnemius muscle morphometry in rats with sciatic nerve injury.**
(A) Representative three-dimensional plantar pressure distributions of the hindlimbs of the injured and healthy sides. There were unambiguous footprints with better toe spread observed in the Chi/PDA-Exos group. (B) Quantification analysis of SFI values 8 weeks after surgery (n = 8 for each group). (C) Representative electromyography 8 weeks after surgery. The CMAP latency of the Chi/PDA-Exos group was shorter than that of the Chi group. The CMAP amplitude of the Chi/PDA-Exos group was higher than that in the Chi and Chi-Exos groups. (D, E) Quantification analysis of CMAP latency (D) and amplitude (E) 8 weeks after surgery (n = 8 for each group). (F) Photographs of the gastrocnemius muscles on both sides 8 weeks after surgery. The muscle volume on the right side was smaller than on the left side for each group. (G) Quantification analysis of muscle wet weight rates of the injured side to the uninjured side (n = 3 for each group). (H) Masson's trichrome staining of transverse sections of the gastrocnemius muscles of the injured limbs. The mean cross-sectional area of the muscle fibers was larger in the Chi/PDA-Exos group than in the Chi and Chi-Exos groups. Scale bars: 50 μm. (I) Quantification analysis of the cross-sectional areas of the gastrocnemius muscle fibers (n = 8 for each group). Data are expressed as mean ± SEM. $^{*}P < 0.05$, $^{**}P < 0.01$, *vs.* Chi group; $^{\#}P < 0.05$, $^{\#\#}P < 0.01$, *vs.* Chi-Exos group (one-way analysis of variance followed by Tukey's *post hoc* test). Chi: Chitin; Chi/PDA: polydopamine-coated chitin conduits; Chi/PDA-Exos: polydopamine-coated chitin conduits loaded with exosomes; Chi-Exos: chitin conduits loaded with exosomes; SFI: sciatic functional index.

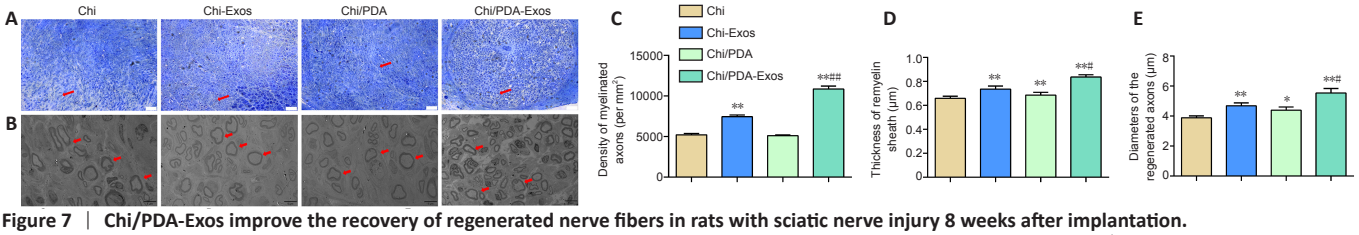

Figure 7 | **Chi/PDA-Exos improve the recovery of regenerated nerve fibers in rats with sciatic nerve injury 8 weeks after implantation.**
(A) Transverse sections of the distal nerve stained with toluidine blue. Nerve axons (red arrows) were evenly distributed in the Chi/PDA-Exos group. (B) Transmission electron microscopy images of the regenerated sciatic nerve. Axons (red arrows) that were evenly distributed and more structurally complete were observed in the Chi/PDA-Exos group. Scale bars: 50 μm (A), 5 μm (B). (C–E) Quantification analysis of density of myelinated axons (C), thickness of the remyelination sheath (D), and diameters of remyelinated axons (E) of regenerated axons. Data are expressed as mean ± SEM (n = 8 for each group). $^{*}P < 0.05$, $^{**}P < 0.01$, *vs.* Chi group; $^{\#}P < 0.05$, $^{\#\#}P < 0.01$, *vs.* Chi-Exos group (one-way analysis of variance followed by Tukey's *post hoc* test). Chi: Chitin; Chi/PDA: polydopamine-coated chitin conduits; Chi/PDA-Exos: polydopamine-coated chitin conduits loaded with exosomes; Chi-Exos: chitin conduits loaded with exosomes.

Exosomes are nano-sized membrane-enclosed vesicles that play a vital role in cell-to-cell communication (Park et al., 2007; Rani et al., 2015). Exosomes can transfer the characteristics and signaling molecules of the parent cells to their target cells and regulate normal physiological functions or disease states of recipient cells (Kourembanas, 2015; Rani and Ritter, 2016; Phinney and Pittenger, 2017). Mesenchymal stem cell-derived exosomes mainly perform biological functions by delivering mRNA, microRNA, and proteins, so they circumvent many risks associated with direct transplantation of stem cells and have great therapeutic potential in the field of cell-free regenerative medicine (Tsiapalis and O'Driscoll, 2020). A previous study found that exosomes derived from BMSCs promoted the functional recovery of sciatic nerve crush injury through a microRNA-mediated mechanism (Zhao et al., 2020). However, peripheral nerve regeneration is complex and involves multiple consecutive and overlapping stages (Scheib and Höke, 2013). A single administration of exosomes into Chi conduits is not sufficient to achieve nerve regeneration because exosomes are easily degraded *in vivo* and the local effective concentration is maintained only for a short time (He et al., 2018; Hessvik and Llorente, 2018).

The phenomenon that mussels can firmly attach to various substrates inspired scientists to discover 3,4-dihydroxy-L-phenylalanine and lysine-enriched proteins. The molecular structure of PDA is similar to 3,4-dihydroxy-L-phenylalanine (Liu et al., 2014). Virtually all types of inorganic and organic substrates could be surface-modified with PDA (Cheng et al., 2019). In this study, we use the spontaneous polymerization of PDA to coat Chi conduits to achieve better loading of biologically active substances. Here, we successfully combined BMSC-Exos and Chi/PDA conduits. BMSC-Exos did not change the microstructure of the Chi conduits. By calculating the remaining exosomes in solution, we estimated the weights of exosomes immobilized to Chi conduits and to PDA-coated Chi conduits were 346.7 ± 8.82 μg and 710 ± 17.32 μg, respectively. Exosomes in the Chi/PDA-Exos group appeared to be released in a sustained manner, while exosomes in Chi conduits were burst released within 2 days. Thus, we speculate that we achieved our initial goal of sustained release of exosomes. PDA immobilizes the exosomes and reduces exosome loss during circulation inside the conduit. The nano-sized PDA layer and exosomes take up negligible space in the conduits, which leaves enough space for axon regeneration.

SCs are critical to facilitate the regeneration of peripheral nerves after injury. In the current study, we found that SCs treated with BMSC-Exos had higher proliferation rates and secretion of neurotrophic factors (nerve growth factor, brain-derived neurotrophic factor, and ciliary neurotrophic factor) and vascular endothelial growth factor. Initially, the number of exosomes released by Chi-Exos was greater than Chi/PDA-Exos. CCK-8 and ELISA results showed that the proliferation ability and secretion function of SCs in the Chi-Exos group were initially better than SCs in the Chi/PDA-Exos group. However, on day 5 after treatment, the sustained-release effect of Chi/PDA-Exos gradually increased, and the proliferation ability and secretion function of SCs in the Chi/PDA-Exos group were better than in the Chi-Exos group. The SC repair program is controlled by transcription factors; the most important of these is Jun (Jessen and Mirsky, 2016). Reverse transcription-polymerase chain reaction results showed that the mRNA levels of Jun and Sox2 were upregulated after internalization of exosomes, while myelinization-associated genes Mbp and Krox20 were significantly decreased, suggesting activation of a progressive transformation of SCs. Meanwhile, the changes in mRNA expression levels also positively correlated to the numbers of internalized exosomes. However, we also found that the SC expression of Mbp and Krox20 was higher in the Chi/PDA-Exos group than in the Chi-Exos group after 5 days of treatment, which may be related to the presence of PDA. The specific mechanisms involved need to be investigated further.

Primary DRGs were treated with exosomes and used to study peripheral nerve regeneration. Previous studies have demonstrated the positive role of exosomes in promoting axon growth in the central nervous system and peripheral nervous system (Court et al., 2011; Bucan et al., 2019). Our data showed that the outgrowth of DRG neurons was improved after treatment with BMSC-derived exosomes for 7 days. Sustained release of exosomes tends to significantly enhance axon growth, which is particularly important for peripheral nerve regeneration (Zhao et al., 2020).

On the basis of the optimal effects of Chi/PDA-Exos conduits *in vitro*, we performed *in vivo* experiments. We found no neuromas formed at suture sites and no obvious inflammation or tissue adhesion occurred around the conduits in all groups. SFI and gait movement results were best in the Chi/PDA-Exos group compared with all other groups. Consistent with previous results, muscle wet weight rate and diameter of muscle fibers were also significantly increased in the Chi/PDA-Exos group, which indicated attenuation of muscle atrophy after peripheral nerve regeneration. Nerve tissue morphology results revealed the morphological restoration of myelination and regularity of nerve bundles, which represent important indicators of peripheral nerve regeneration (Modrak et al., 2020).

Exosomes can continue to affect the repair phenotype of SCs, which in turn, affect the remyelination process. However, our experimental results did not show obvious inhibition of remyelination. In the later stage of repair, a greater number of SCs in the injured area may help the functional recovery of regenerated nerves (Jessen and Mirsky, 2016). Our results reflect this possibility and suggest that we have constructed a sustained exosome-release system to enhance repair by SCs. A limitation of this study is that we only investigated the effects of Chi/PDA-Exos on peripheral nerve regeneration for up to 8 weeks after surgery. The long-term effects should be investigated in further studies. The differences between healthy nerves and regenerated nerves should also be observed. In the future, we will study this sustained-release exosome-based system in long-distance peripheral nerve defects and investigate associated molecular mechanisms.

To conclude, we successfully constructed an efficient adhesion strategy for exosomes by coating Chi conduits with a nano-sized PDA layer. This newly designed system allowed sustained release of exosomes. Exosomes can activate and maintain the repair phenotype of SCs, thereby providing a better microenvironment for nerve regeneration. Our results indicate that our adhesion strategy may have great practical value for exosome-based treatments and personalized medical research.

Acknowledgments: *We are grateful for the assistance of BioRender.com with some pictures.*
Author contributions: *Study design and support, and manuscript revision: PXZ; data analysis and manuscript draft: CL, SYL; experiment implementation: MZ, WP, BW, QCL, CFL. All authors contributed to the article and approved the submitted version.*
Conflicts of interest: *The authors have declared that no competing interest exists.*
Availability of data and materials: *All data generated or analyzed during this study are included in this published article and its supplementary information files.*

Open peer reviewer: *Maria Easler, University of Padova, Italy.*
Additional file: *Open peer review report 1.*

References

Bucan V, Vaslaitis D, Peck CT, Strauß S, Vogt PM, Radtke C (2019) Effect of exosomes from rat adipose-derived mesenchymal stem cells on neurite outgrowth and sciatic nerve regeneration after crush injury. Mol Neurobiol 56:1812-1824.

Castelnovo LF, Thomas P, Magnaghi V (2021) Membrane progesterone receptors (mPRs/PAQRs) in Schwann cells represent a promising target for the promotion of neuroregeneration. Neural Regen Res 16:281-282.

Cheng W, Zeng X, Chen H, Li Z, Zeng W, Mei L, Zhao Y (2019) Versatile polydopamine platforms: synthesis and promising applications for surface modification and advanced nanomedicine. ACS Nano 13:8537-8565.

Court FA, Midha R, Cisterna BA, Grochmal J, Shakhbazau A, Hendriks WT, Van Minnen J (2011) Morphological evidence for a transport of ribosomes from Schwann cells to regenerating axons. Glia 59:1529-1539.

Gnecchi M, He H, Liang OD, Melo LG, Morello F, Mu H, Noiseux N, Zhang L, Pratt RE, Ingwall JS, Dzau VJ (2005) Paracrine action accounts for marked protection of ischemic heart by Akt-modified mesenchymal stem cells. Nat Med 11:367-368.

He C, Zheng S, Luo Y, Wang B (2018) Exosome theranostics: biology and translational medicine. Theranostics 8:237-255.

Hessvik NP, Llorente A (2018) Current knowledge on exosome biogenesis and release. Cell Mol Life Sci 75:193-208.

Jessen KR, Mirsky R (2016) The repair Schwann cell and its function in regenerating nerves. J Physiol 594:3521-3531.

Jessen KR, Arthur-Farraj P (2019) Repair Schwann cell update: adaptive reprogramming, EMT, and stemness in regenerating nerves. Glia 67:421-437.

Jiang B, Liang S, Peng ZR, Cong H, Levy M, Cheng Q, Wang T, Remais JV (2017) Transport and public health in China: the road to a healthy future. Lancet 390:1781-1791.

Kourembanas S (2015) Exosomes: vehicles of intercellular signaling, biomarkers, and vectors of cell therapy. Annu Rev Physiol 77:13-27.

Kovacic U, Sketelj J, Bajrović FF (2003) Sex-related difference in collateral sprouting of nociceptive axons after peripheral nerve injury in the rat. Exp Neurol 184:479-488.

Lee H, Dellatore SM, Miller WM, Messersmith PB (2007) Mussel-inspired surface chemistry for multifunctional coatings. Science 318:426-430.

Li C, Liu SY, Pi W, Zhang PX (2021) Cortical plasticity and nerve regeneration after peripheral nerve injury. Neural Regen Res 16:1518-1523.

Li C, Jiao G, Wu W, Wang H, Ren S, Zhang L, Zhou H, Liu H, Chen Y (2019) Exosomes from bone marrow mesenchymal stem cells inhibit neuronal apoptosis and promote motor function recovery via the Wnt/β-catenin signaling pathway. Cell Transplant 28:1373-1383.

Liu Y, Ai K, Lu L (2014) Polydopamine and its derivative materials: synthesis and promising applications in energy, environmental, and biomedical fields. Chem Rev 114:5057-5115.

Lu CF, Wang B, Zhang PX, Han S, Pi W, Kou YH, Jiang BG (2021) Combining chitin biological conduits with small autogenous nerves and platelet-rich plasma for the repair of sciatic nerve defects in rats. CNS Neurosci Ther 27:805-819.

Lu PJ, Wang G, Cai XD, Zhang P, Wang HK (2020) Sequencing analysis of matrix metalloproteinase 7-induced genetic changes in Schwann cells. Neural Regen Res 15:2116-2122.

Milane L, Singh A, Mattheolabakis G, Suresh M, Amiji MM (2015) Exosome mediated communication within the tumor microenvironment. J Control Release 219:278-294.

Modrak M, Talukder MAH, Gurgenashvili K, Noble M, Elfar JC (2020) Peripheral nerve injury and myelination: Potential therapeutic strategies. J Neurosci Res 98:780-795.

Nocera G, Jacob C (2020) Mechanisms of Schwann cell plasticity involved in peripheral nerve repair after injury. Cell Mol Life Sci 77:3977-3989.

Pabari A, Yang SY, Seifalian AM, Mosahebi A (2010) Modern surgical management of peripheral nerve gap. J Plast Reconstr Aesthet Surg 63:1941-1948.

Park H, Temenoff JS, Tabata Y, Caplan AI, Mikos AG (2007) Injectable biodegradable hydrogel composites for rabbit marrow mesenchymal stem cell and growth factor delivery for cartilage tissue engineering. Biomaterials 28:3217-3227.

Peixun Z, Na H, Kou Y, Xiaofeng Y, Jiang B (2017) Peripheral nerve intersectional repair by bi-directional induction and systematic remodelling: biodegradable conduit tubulization from basic research to clinical application. Artif Cells Nanomed Biotechnol 45:1464-1466.

Phinney DG, Pittenger MF (2017) Concise review: MSC-derived exosomes for cell-free therapy. Stem Cells 35:851-858.

Phinney DG, Di Giuseppe M, Njah J, Sala E, Shiva S, St Croix CM, Stolz DB, Watkins SC, Di YP, Leikauf GD, Kolls J, Riches DW, Deiuliis G, Kaminski N, Boregowda SV, McKenna DH, Ortiz LA (2015) Mesenchymal stem cells use extracellular vesicles to outsource mitophagy and shuttle microRNAs. Nat Commun 6:8472.

Qian Y, Zhao X, Han Q, Chen W, Li H, Yuan W (2018) An integrated multi-layer 3D-fabrication of PDA/RGD coated graphene loaded PCL nanoscaffold for peripheral nerve restoration. Nat Commun 9:323.

Qu WR, Zhu Z, Liu J, Song DB, Tian H, Chen BP, Li R, Deng LX (2021) Interaction between Schwann cells and other cells during repair of peripheral nerve injury. Neural Regen Res 16:93-98.

Rani S, Ritter T (2016) The exosome- a naturally secreted nanoparticle and its application to wound healing. Adv Mater 28:5542-5552.

Rani S, Ryan AE, Griffin MD, Ritter T (2015) Mesenchymal stem cell-derived extracellular vesicles: toward cell-free therapeutic applications. Mol Ther 23:812-823.

Rao F, Yuan Z, Zhang D, Yu F, Li M, Li D, Jiang B, Wen Y, Zhang P (2019) Small-molecule SB216763-loaded microspheres repair peripheral nerve injury in small gap tubulization. Front Neurosci 13:489.

Rao F, Wang Y, Zhang D, Lu C, Cao Z, Sui J, Wu M, Zhang Y, Pi W, Wang B, Kou Y, Wang X, Zhang P, Jiang B (2020) Aligned chitosan nanofiber hydrogel grafted with peptides mimicking bioactive brain-derived neurotrophic factor and vascular endothelial growth factor repair long-distance sciatic nerve defects in rats. Theranostics 10:1590-1603.

Salzer JL (2015) Schwann cell myelination. Cold Spring Harb Perspect Biol 7:a020529.

Scheib J, Höke A (2013) Advances in peripheral nerve regeneration. Nat Rev Neurol 9:668-676.

Schneider CA, Rasband WS, Eliceiri KW (2012) NIH Image to ImageJ: 25 years of image analysis. Nat Methods 9:671-675.

Schmittgen TD, Livak KJ (2008) Analyzing real-time PCR data by the comparative C(T) method. Nat Protoc 3:1101-1108.

Sensharma P, Madhumathi G, Jayant RD, Jaiswal AK (2017) Biomaterials and cells for neural tissue engineering: Current choices. Mater Sci Eng C Mater Biol Appl 77:1302-1315.

Timmers L, Lim SK, Arslan F, Armstrong JS, Hoefer IE, Doevendans PA, Piek JJ, El Oakley RM, Choo A, Lee CN, Pasterkamp G, de Kleijn DP (2007) Reduction of myocardial infarct size by human mesenchymal stem cell conditioned medium. Stem Cell Res 1:129-137.

Tsiapalis D, O'Driscoll L (2020) Mesenchymal stem cell derived extracellular vesicles for tissue engineering and regenerative medicine applications. Cells 9:991.

Valadi H, Ekström K, Bossios A, Sjöstrand M, Lee JJ, Lötvall JO (2007) Exosome-mediated transfer of mRNAs and microRNAs is a novel mechanism of genetic exchange between cells. Nat Cell Biol 9:654-659.

Xiao S, Xiao C, Miao Y, Wang J, Chen R, Fan Z, Hu Z (2021) Human acellular amniotic membrane incorporating exosomes from adipose-derived mesenchymal stem cells promotes diabetic wound healing. Stem Cell Res Ther 12:255.

Zhang L, Jiao G, Ren S, Zhang X, Li C, Wu W, Wang H, Liu H, Zhou H, Chen Y (2020) Exosomes from bone marrow mesenchymal stem cells enhance fracture healing through the promotion of osteogenesis and angiogenesis in a rat model of nonunion. Stem Cell Res Ther 11:38.

Zhang P, Han N, Wang T, Xue F, Kou Y, Wang Y, Yin X, Lu L, Tian G, Gong X, Chen S, Dang Y, Peng J, Jiang B (2013) Biodegradable conduit small gap tubulization for peripheral nerve mutilation: a substitute for traditional epineurial neurorrhaphy. Int J Med Sci 10:171-175.

Zhang PX, Li-Ya A, Kou YH, Yin XF, Xue F, Han N, Wang TB, Jiang BG (2015) Biological conduit small gap sleeve bridging method for peripheral nerve injury: regeneration law of nerve fibers in the conduit. Neural Regen Res 10:71-78.

Zhang PX, Han N, Kou YH, Zhu QT, Liu XL, Quan DP, Chen JG, Jiang BG (2019) Tissue engineering for the repair of peripheral nerve injury. Neural Regen Res 14:51-58.

Zhao J, Ding Y, He R, Huang K, Liu L, Jiang C, Liu Z, Wang Y, Yan X, Cao F, Huang X, Peng Y, Ren R, He Y, Cui T, Zhang Q, Zhang X, Liu Q, Li Y, Ma Z, et al. (2020) Dose-effect relationship and molecular mechanism by which BMSC-derived exosomes promote peripheral nerve regeneration after crush injury. Stem Cell Res Ther 11:360.

P-Reviewer: Easler M; C-Editor: Zhao M; S-Editors: Yu J, Li CH; L-Editors: Yu J, Song LP; T-Editor: Jia Y